Carbon 122 (2017) 162–167

Contents lists available at ScienceDirect

Carbon

journal homepage: www.elsevier.com/locate/carbon

Biocompatible carbon nanotube fibers for implantable supercapacitors

Sisi He [a, 1], Yajie Hu [a, 1], Jiaxun Wan [a], Qiang Gao [a, b], Yuhang Wang [c], Songlin Xie [a], Longbin Qiu [a], Changchun Wang [a], Gengfeng Zheng [c], Bingjie Wang [a, d, **], Huisheng Peng [a, *]

[a] State Key Laboratory of Molecular Engineering of Polymers, Department of Macromolecular Science and Laboratory of Advanced Materials, Fudan University, Shanghai 200438, China
[b] Key Laboratory of Science and Technology of Eco-Textiles, Ministry of Education, Jiangnan University, Wuxi 214122, China
[c] Laboratory of Advanced Materials, Department of Chemistry, Collaborative Innovation Center of Chemistry for Energy Materials, Fudan University, Shanghai 200433, China
[d] Ningguo Long Sheng Flexible Energy Storage Materials Technology Co., LTD, China

ARTICLE INFO

Article history:
Received 30 March 2017
Received in revised form
3 June 2017
Accepted 19 June 2017
Available online 22 June 2017

Keywords:
Biocompatible
Hydrophilic
Carbon nanotube
Supercapacitor
Implantable

ABSTRACT

The rapid advances in implantable electronic medical devices make supercapacitors highly desirable as power sources. These supercapacitors should be biocompatible, lightweight, miniature and stable without the need for packaging, which unfortunately remains unavailable yet. Here a new family of biocompatible carbon nanotube fibers were synthesized as electrodes to fabricate new supercapacitors that could directly work in physiological fluids including phosphate buffer saline, serum and blood with high energy storage capabilities. For instance, the specific capacitance reached 10.4 F/cm^3 or 20.8 F/g that could be maintained by 98.3% after 10,000 cycles in phosphate buffer saline.

1. Introduction

The rapid development of the flexible electronics opens up a variety of promising applications in biomedical fields such as monitoring biological signals including electrocardiogram, thermal, mechanical and electrophysiological information [1–3]. Among them, the appearance of implantable flexible electronic devices provides an efficient strategy to monitor health conditions inside the biological body [4–7]. To this end, it is critical to find matchable power systems that are supposed to be also biocompatible and implantable [8–10]. Supercapacitors with high power densities have been thus proposed as promising candidates to power the implantable electronic devices [11,12]. However, the conventional supercapacitors cannot well meet the above requirements. For instance, they are generally rigid and heavy, which is unsuitable for portable and flexible devices; the used electrolyte is unstable, so they need strict encapsulation, which makes surgery operations complex and the patients painful; the complex and rigid encapsulation also limits the miniaturization of the supercapacitors. One possible strategy is taking advantage of body fluid directly as electrolyte to avoid the encapsulation.

Carbon nanotube (CNT) materials, especially aligned CNT fibers, are recently studied for light weight, high flexibility, and excellent mechanical and electronic properties [13–16]. However, their hydrophobic nature has limited their applications in biomedical field. For instance, the anisotropic structure of aligned CNTs could be used to guide the growth and differentiation of cells in various tissues, but the poor interaction between hydrophobic CNTs and cells largely decreased cell attachment and growth rate [17,18]. Besides, their large specific surface areas and high electrical conductivities made them promising as electrodes in fabricating energy storage devices such as supercapacitors, but their poor wettability to the electrolyte that was typically hydrophilic led to a relatively low energy density [19].

Here we developed a neat and effective strategy to continuously

* Corresponding author.
** Corresponding author.State Key Laboratory of Molecular Engineering of Polymers, Department of Macromolecular Science and Laboratory of Advanced Materials, Fudan University, Shanghai 200438, China
E-mail address: penghs@fudan.edu.cn (H. Peng).
[1] These authors contributed equally to this work.

http://dx.doi.org/10.1016/j.carbon.2017.06.053
0008-6223/

synthesize biocompatible CNT fibers as effective electrodes for novel supercapacitors with physiological fluids including phosphate buffered saline (PBS), serum and blood directly acting as electrolytes (Fig. 1(a)). The specific capacitance reached 10.4 F/cm^3 or 20.8 F/g that could be maintained by 98.3% after 10,000 cycles.

2. Experimental section

2.1. Synthesis of hydrophilic aligned CNTs

Spinnable CNT arrays were grown in a tube furnace for 10–20 min by chemical vapor deposition, and they were then treated by an oxygen microwave plasma (Plasma System 690, PVA Tepla). The treated power was tuned from 50 to 200 W under a fixed time of 10 min with a pressure of 0.1 mbar and a flow rate of oxygen gas of 300 sccm. Hydrophilic CNT sheets were directly drawn from the modified CNT arrays, and the hydrophilic CNT fibers were prepared by the following twisting of the hydrophilic sheets at a rotary speed of 200 revolutions per minute. The CNT fibers were wound on a collecting drum with a speed of 15 cm per minute.

2.2. Cell culture and characterization

NIH-3T3 cells were cultured in Dulbecco's modification of Eagle's medium supplied with 10% fetal bovine serum, 100 U/ml penicillin and 0.1 mg/mL streptomycin. They were incubated at 37 °C in a humidified environment containing 5% CO_2, and the culture medium was changed every three days. The NIH-3T3 cells were fixed in a 4% paraformaldehyde solution in PBS solution for 5–10 min. Next, they were treated with 1% bovine serum albumin in PBS solution to block nonspecific binding sites for 30 min. After washing with PBS solution, the NIH-3T3 cells were stained with the phalloidin-fluorescein isothiocyanate and Hoechst 33342 to label F-action and cell nucleus. Finally, they were imaged by laser confocal scanning microscopy (LSM710, Carl Zeiss, Germany) and fluorescence microscopy (BX51, Olympus, Japan). NIH-3T3 cells were fixed at 2.5% glutaraldehyde in phosphate-buttered saline for 4 h at 4 °C. After washing with water for three times, they were dehydrated by 20% dimethylsulfoxide in water for 4 h and dried in critical point dryer, followed by coating platinum using a sputter coater. The samples were observed under a field emission scanning electron microscopy operated at 3.0 kV (Ultra 55, Carl Zeiss, Germany). Serum and blood came from mice (BALB/c, male, 6–7 weeks) that provided by Shanghai Laboratory Animal Centre and acclimatized under standard conditions, with a 12 h light/dark cycle.

3. Result and discussion

To synthesize biocompatible CNT fibers, spinnable CNT arrays were firstly synthesized by chemical vapor deposition [20], followed by oxygen plasma treatment (Fig. 1(b–d)). During the oxygen plasma treatment, atomic oxygen species, which were produced by breaking the binding energy of covalent bonds in

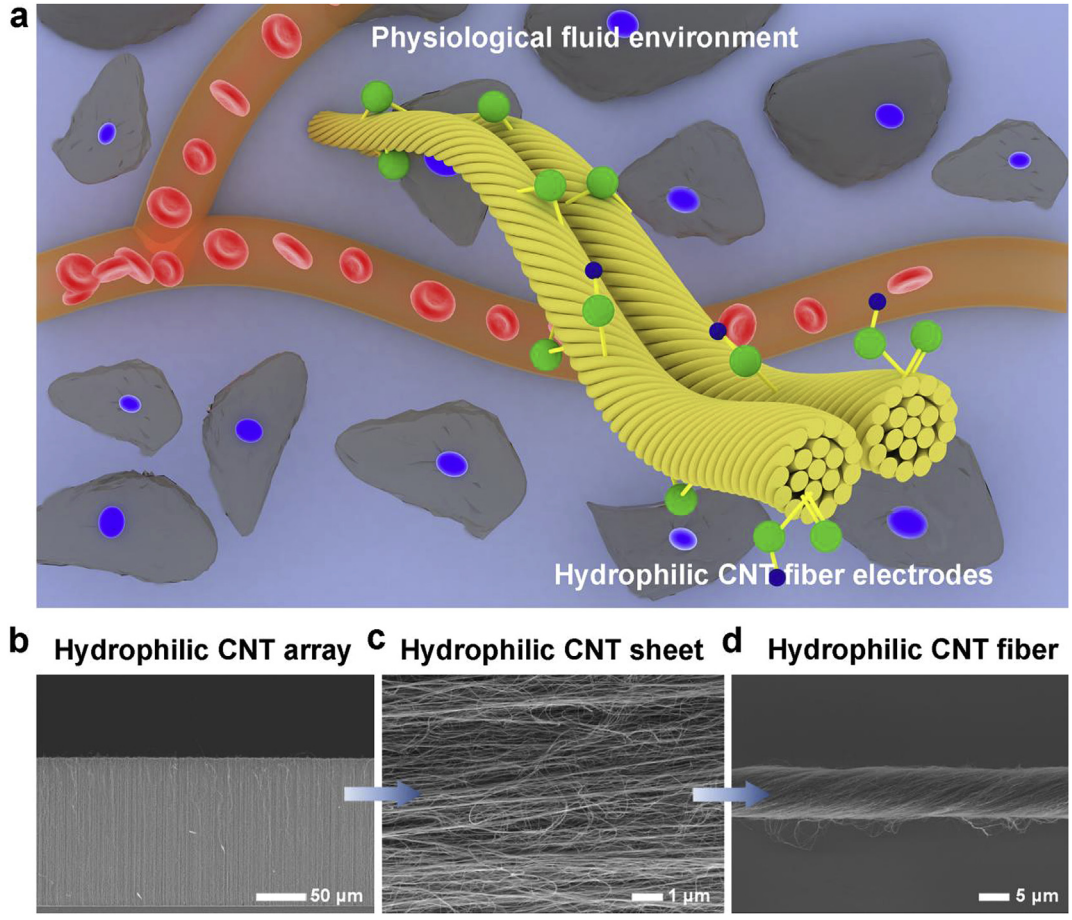

Fig. 1. Biocompatible supercapacitor in the physiological fluids. **(a)** Schematic illustration to the hydrophilic CNT fiber as two electrodes to fabricate fiber-shaped supercapacitor in the physiological fluids. **(b–d)** Photographs of spinnable hydrophilic CNT array, pulled CNT sheet and twisted CNT fiber, respectively. (A colour version of this figure can be viewed online.)

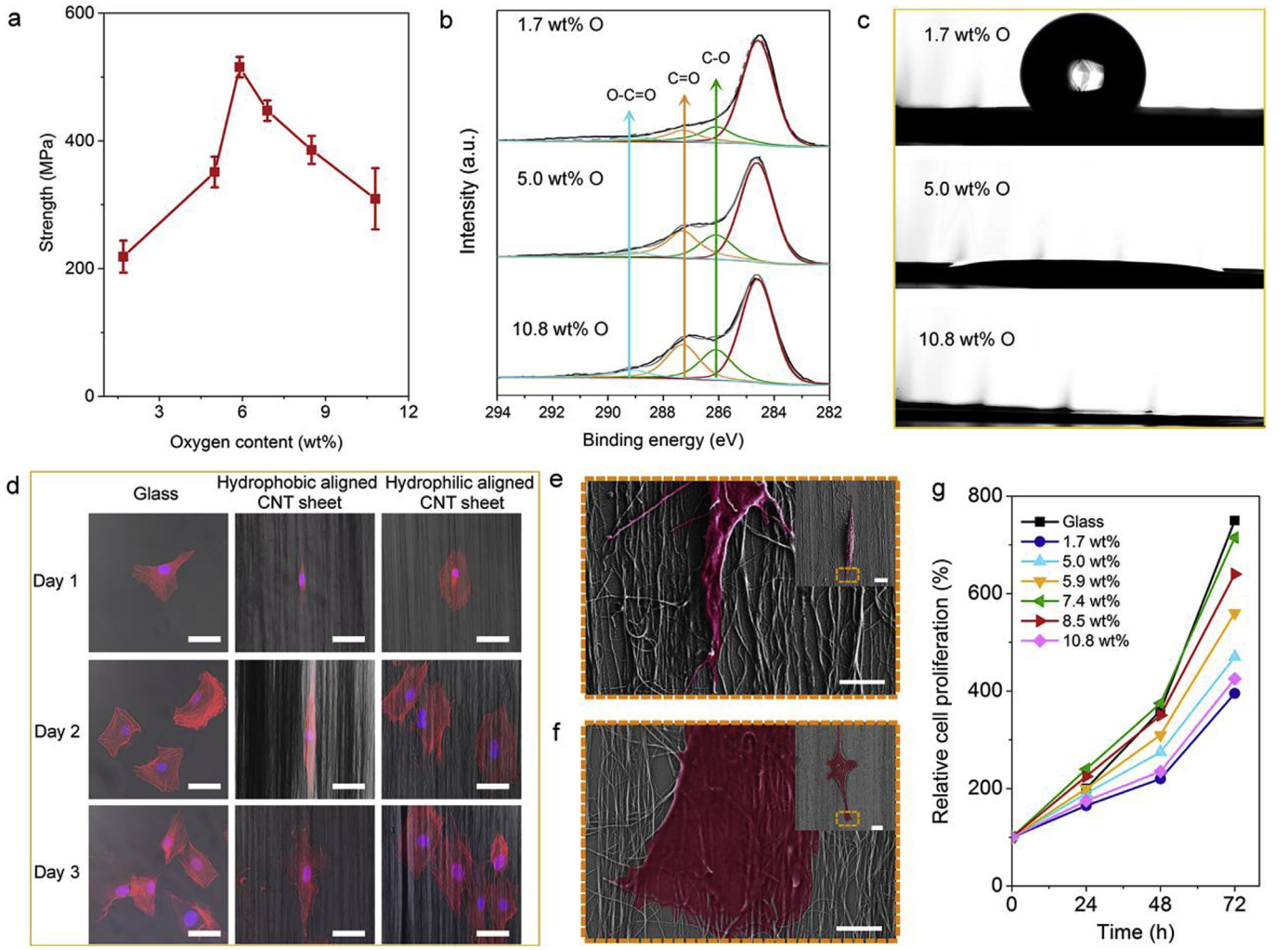

Fig. 2. Property and biocompatibility of the hydrophilic CNT electrode. **(a)** Dependence of tensile strength of hydrophilic CNT fiber on oxygen content. **(b)** XPS C1s binding energy regions of hydrophilic CNTs with increasing oxygen contents. **(c)** Photographs showing the contact angles of water droplets on hydrophilic CNTs with increasing oxygen contents. **(d)** Fluorescent images of the actin cytoskeleton (red) and the core (blue) of NIH-3T3 cells cultured on glass, hydrophobic CNTs and hydrophilic CNTs at Day 1, 2 and 3. **(e** and **f)** SEM images of the NIH-3T3 cell cultured on the hydrophobic and hydrophilic CNTs, respectively (inserted, corresponding fluorescent image). **(g)** Dependence of cell proliferation on culture time above hydrophilic CNTs with increasing oxygen contents. Scale bar at d, 50 μm; scale bar at e and f, 2 μm (inserted image, 10 μm). (A colour version of this figure can be viewed online.)

oxygen molecule, reacted with CNTs to generate oxygen-containing groups (Fig. S1). These hydrophilic CNTs exhibited multi-walled structures with an average diameter of ~10 nm (Fig. S2). Note that the oxygen plasma did not decrease the alignment of CNTs (Fig. 1(b)), so the hydrophilic CNT arrays were also spinnable. CNT sheets were directly drawn from the hydrophilic arrays and further twisted to produce CNT fibers (Fig. 1(d)).

The oxygen content could be controlled from 1.7 to 10.8 wt% by varying the reaction parameters such as applied power and reaction time (Fig. S3). Spinnable hydrophilic CNT arrays with increasing oxygen contents from 1.7 to 5.9 wt% under the increasing power ranging from 0 to 100 W were mainly prepared from the typical CNT arrays with the height of 224 μm. A poor spinnability was observed at the treatment power above 100 W because the top parts of the CNTs were etched with the decreasing height (Fig. S4). The resulting low CNT array was not able to form a pulling-out process owing to the limited interconnections among neighboring CNT bundles [21]. To this end, spinnable hydrophilic CNT arrays with higher oxygen contents from 5.9 to 10.8 wt% were synthesized from taller array precursors (i.e., 400 μm) at higher powers from 100 to 200 W. In fact, the top part of the CNT array became much more disordered and entangled (Fig. S6). It was thus difficult to continuously pull out of the neighboring CNT bundles based on the top-to-bottom spinning mechanism [8].

Importantly, the mechanical properties of CNT fibers were enhanced after oxygen plasma treatment also with high electrical conductivities. The tensile strengths of the CNT fibers increased from 218.6 to 515.4 MPa with the increasing oxygen contents from 1.7 to 5.9 wt% due to the formation of increasing hydrogen bonds among neighboring CNTs (Fig. 2(a)); it started to gradually reduce beyond 5.9%, e.g., 309.1 MPa at 10.8 wt%, as the produced more defects overstepped the hydrogen bonds. The formation of oxygen-containing groups introduced attractive bindings among neighboring CNTs but also decreased the integrity of CNTs (Fig. S7) [22,23]. Nevertheless, the hydrophilic CNT fibers exceeded the previous hydrophobic counterparts in tensile strength. Electrical conductivities of CNT fibers were reduced with the increasing oxygen content to 5.9% and remained almost unchanged beyond this point (Fig. S8). The electrical resistance of a CNT fiber mainly came from the contact resistances among neighboring CNTs as the

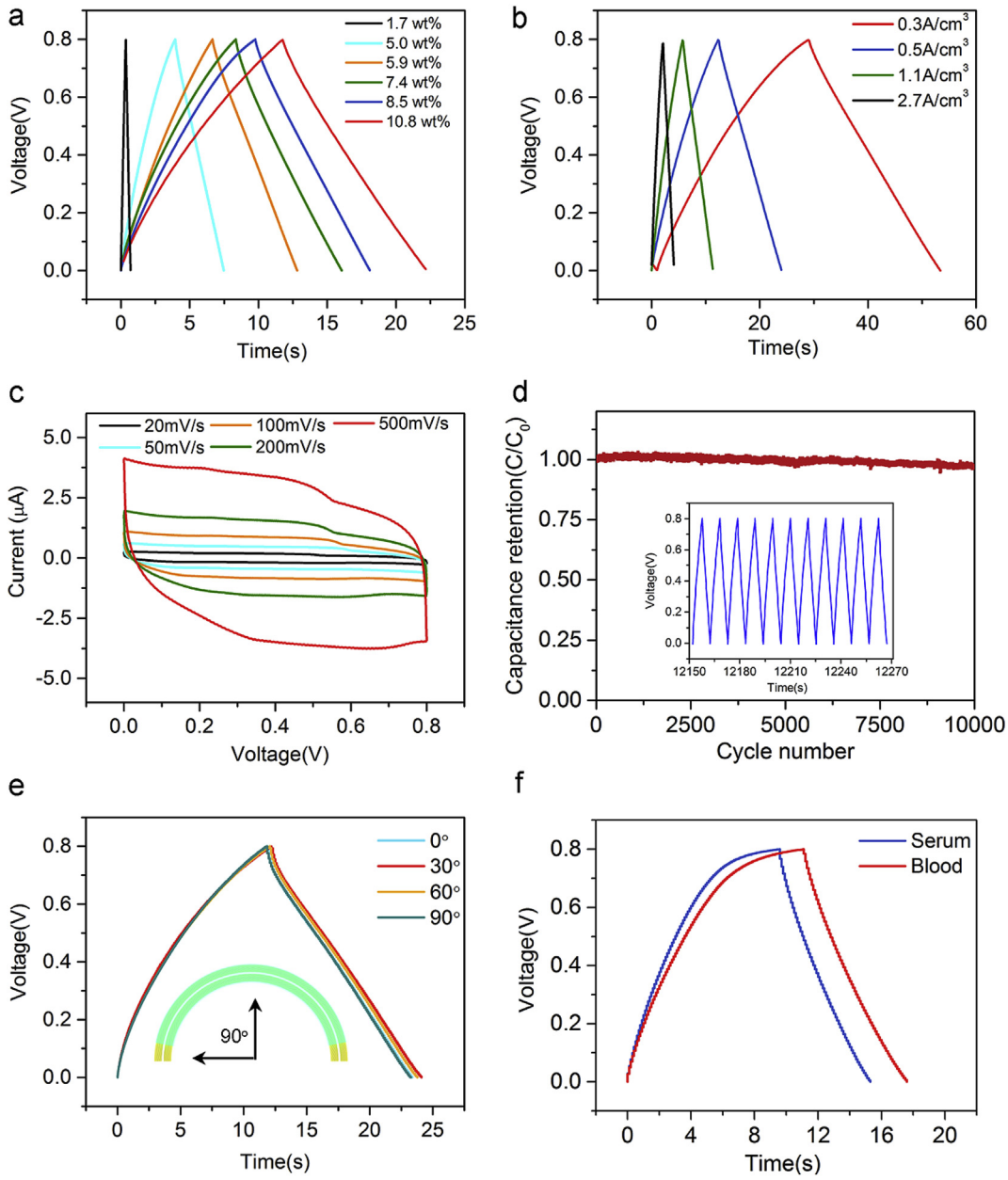

Fig. 3. Performance of the biocompatible supercapacitor in the physiological fluid. **(a)** Galvanostatic charge-discharge curves with increasing oxygen contents from 1.7 to 10.8 wt% at a current density of 0.5 A/cm^3 in PBS solution. **(b)** Galvanostatic charge-discharge curves of a 10.8 wt% oxygen supercapacitor with increasing current densities from 0.3 to 2.7 A/cm^3 in PBS solution. **(c)** Cyclic voltammograms of a 10.8 wt% oxygen supercapacitor with increasing scan rates from 20 to 500 mV/s in PBS solution. **(d)** Cyclic performance of a 10.8 wt% oxygen supercapacitor in PBS solution. **(e)** Dependence of capacitance retention on bending angle at a current density of 0.5 A/cm^3 in PBS solution. **(f)** Galvanostatic charge-discharge curves of a 10.8 wt% oxygen supercapacitor in serum and blood at a current density of 0.5 A/cm^3 in serum and blood. (A colour version of this figure can be viewed online.)

resistances of individual CNTs were much lower, while both oxygen-containing groups and defects increased their contact resistances.

The CNT atomic structures were further traced with the increasing oxygen content by X-ray photoelectron spectroscopy (Fig. 2(b) and Fig. S9). The O 1s spectrum revealed several oxygen species including hydroxyl (C–O, 286.3 eV), carbonyl (C=O, 287.5 eV) and carboxylic (O–C=O, 298.1 eV). Besides the main feature of the sp^2 bond (C=C, 284.8 eV), the primary C 1s peak also displayed characteristic peaks of oxygen-containing functional groups. The oxygen-containing functional groups obviously increased with the increasing power or treating time. Accordingly, the increasing hydrophilicity was verified by the increasing water contact angle (Fig. 2(c) and Fig. S10).

To investigate the biocompatibility of hydrophilic CNTs, we cultured NIH-3T3 fibroblast cells on them with the hydrophobic counterpart and glass as two control samples. The NIH-3T3 cells were all alive on the hydrophilic CNTs after 24 h (Fig. S11). In contrast, the viability was lower for the hydrophobic CNTs. The enhanced biocompatibility of the hydrophilic CNTs was also verified by lactate dehydrogenase test (Fig. S12). No significant lactate dehydrogenase release was found for the hydrophilic CNTs, whereas it was twice of that for the hydrophobic CNTs. The cell proliferation evaluated from a Cell Counting Kit-8 assay was much

better on the hydrophilic CNTs compared with the two kinds of control samples (Fig. S13).

The hydrophilic surface of CNTs was the critical factor for cell growth, and a comparing culture study was made for one, two and three days (Fig. 2(d)). With the assistance of staining F-actin filament with phalloidin-fluorescein isothiocyanate and cell nuclei with Hoechst 33342, we found that the cultured cells on the hydrophilic CNTs appeared with a broader spindle shape. Scanning electron microscopy (SEM) also verified that the NIH-3T3 cells on the hydrophobic CNTs exhibited filopodia extensions at ends, and these filopodia extensions grew along the CNT-aligned direction (Fig. 2(e) and (f)). They were composed of actin filaments and acted to sense and navigate the environment [24]. Differently, there were lamellipodia extensions at the cell ends on the hydrophilic CNTs (Fig. 2(e)). The hydrophilic CNTs with increasing oxygen contents had been further quantitatively compared. The cell proliferation was investigated by cell number counting after cell culture for 72 h (Fig. 2(g) and S14). The cell numbers increased with the increasing culture time for all hydrophilic CNTs, and the proliferation rates further increased on the hydrophilic ones with increasing oxygen contents. The increasing hydrophilic surface offered a better sensitivity for cells to the surface morphology through the lamellipodia extensions [25,26].

Two biocompatible CNT fibers were further twisted into a fiber-shaped supercapacitor that worked by using a physiological fluid as the electrolyte. Brunauer–Emmett–Teller (BET) analysis showed that CNTs had a specific surface area of 395 m^2/g (Fig. S15). The galvanostatic charge/discharge curves were firstly studied by assembling a supercapacitor in PBS electrolyte. The fiber-shaped supercapacitors with increasing oxygen contents were compared at a current density of 0.5 A/cm^3, and the results are shown in Fig. 3(a). The discharge time was increased with the increasing oxygen contents, showing an enhanced electrochemical performance. An oxygen content of 10.8 wt% produced the highest specific capacitance of 10.4 F/cm^3 (20.8 F/g), almost 30 times higher than the hydrophobic CNT fiber (i.e., 0.35 F/cm^3 or 0.7 F/g). The specific capacitance displays a higher value compared with the reported fiber-shaped supercapacitors based on carbon nanotubes, such as 1.58 F/cm^3 for those with a spring-like structure or 4.5 F/g with a twisted structure [27,28].

The greatly enhanced energy storage capability was derived from the oxygen-containing groups on the surface of the hydrophilic CNT fiber by introducing a high pseudocapacitance although the resistance of the hydrophilic CNT fiber increased. Fig. S16 shows the cyclic voltammograms of the hydrophilic fibers with different oxygen contents in 1 M H_2SO_4. Reversible cathodic and anodic peaks were shared for all fiber electrodes, indicating the presence of pseudocapacitance. The above peaks became larger in area for higher pseudocapacitances with increasing oxygen contents from 1.7 to 10.8 wt% [29]. In contrast, the redox peaks disappeared in 1 M $LiClO_4$, a neutral electrolyte, so the pseudocapacitance was ascribed to the oxygen-containing groups (Fig. S17) [30]. Fig. S18 shows the impedance measurements of the capacitors made by the hydrophilic fibers with different oxygen contents. With the increase of oxygen contents, the impedance of the capacitors decreased owing to the better hydrophilicity of the fibers and thus higher contact angles with the electrolyte. As the oxygen contents further increased, the impedance of the capacitors slightly increased owing to the increase of the resistance of the hydrophilic CNT fiber. However, although the increase of oxygen contents for performance improvement was expected, the spinnability had been greatly decreased when the oxygen content exceeded 10.8 wt% possibly due to the existence of a large amount of oxygen-containing groups in neighboring CNTs (Fig. S5).

The hydrophilic CNT fiber with an oxygen content of 10.8 wt% was selected as the typical electrode for the supercapacitor to further investigate its electrochemical performances. The galvanostatic charge/discharge curves exhibited a symmetrical shape at increasing current densities of 0.3–2.7 A/cm^3 in PBS, indicating a stable capacitive behavior (Fig. 3(b)) [31]. Similarly, cyclic voltammograms were well maintained under increasing scan rates from 20 to 500 mV/s (Fig. 3(c)), which also verified a high performance during the rapid charge-discharge process and low resistance [32]. The stable capacitive performance was demonstrated by the long cyclic test, and the specific capacitance retained by 98.3% after 10,000 cycles (Fig. 3(d)). The resulting supercapacitors were flexible, and the specific capacitances remained almost unchanged after bending (Fig. 3(e)).

We also investigated the electrochemical properties in serum and blood (Fig. 3(f)). It functioned well in these fluids, and the specific capacitances in serum and blood were 11.4 and 13 F/g, respectively, which were both significantly improved compared with the case of hydrophobic fiber. The hydrophilic CNT fibers also showed stable capacitive behaviors in serum and blood (Fig. S19 and S20).

4. Conclusion

In summary, a new family of hydrophilic CNT fibers was synthesized for biocompatible supercapacitors that worked in a physiological fluid such as PBS, serum and blood. The specific capacitance of the supercapacitor had been maintained by 98.3% even after 10,000 cycles. These biocompatible fiber-shaped supercapacitors were lightweight, flexible and miniature, and they could be further woven into soft electronic textiles aiming at a large-scale application. This work also provides a general and promising strategy in the development of new energy materials and devices.

Acknowledgements

This work was supported by MOST (2016YFA0203302), NSFC (21634003, 51573027, 51403038, 51673043, 21604012, 21474017) and STCSM (16JC1400702, 15XD1500400, 15JC1490200). The sample fabrication was performed at the Fudan Nano-fabrication Laboratory.

Appendix A. Supplementary data

Supplementary data related to this article can be found at http://dx.doi.org/10.1016/j.carbon.2017.06.053.

References

[1] W. Gao, S. Emaminejad, H.Y. Nyein, S. Challa, K. Chen, A. Peck, et al., Fully integrated wearable sensor arrays for multiplexed in situ perspiration analysis, Nature 529 (2016) 509–514.
[2] S.R. Steinhubl, E.D. Muse, E.J. Topol, The emerging field of mobile health, Sci. Transl. Med. 7 (2015), 283rv283.
[3] J. Kim, G.A. Salvatore, H. Araki, A.M. Chiarelli, Z. Xie, A. Banks, et al., Battery-free, stretchable optoelectronic systems for wireless optical characterization of the skin, Sci. Adv. 2 (2016) e1600418.
[4] J. Liu, T.M. Fu, Z. Cheng, G. Hong, T. Zhou, L. Jin, et al., Syringe-injectable electronics, Nat. Nanotechnol. 10 (2015) 629–636.
[5] G. Hong, T.M. Fu, T. Zhou, T.G. Schuhmann, J. Huang, C.M. Lieber, Syringe Injectable electronics: precise targeted delivery with quantitative input/output connectivity, Nano Lett. 15 (2015) 6979–6984.
[6] C. Jin, J. Zhang, X.K. Li, X.Y. Yang, J.J. Li, J. Liu, Injectable 3-D fabrication of medical electronics at the target biological tissues, Sci. Rep. 3 (2013) 3442.
[7] A. Chortos, J. Liu, Z. Bao, Pursuing prosthetic electronic skin, Nat. Mater. 15 (2016) 937–950.
[8] C. Wang, C. Zhao, R. Vijayaraghavan, D.R. MacFarlane, M. Forsyth, G.G. Wallace, Biocompatible ionic liquid-biopolymer electrolyte-enabled thin and compact magnesium-air batteries, ACS Appl. Mater. Interfaces 6 (2014) 21110–21117.
[9] L. Yin, X. Huang, H. Xu, Y. Zhang, J. Lam, J. Cheng, et al., Materials, designs, and

operational characteristics for fully biodegradable primary batteries, Adv. Mater. 26 (2014) 3879–3884.
[10] M. Muskovich, C.J. Bettinger, Biomaterials-based electronics: polymers and interfaces for biology and medicine, Adv. Healthc. Mater. 1 (2012) 248–266.
[11] P. Simon, Y. Gogotsi, Materials for electrochemical capacitors, Nat. Mater. 7 (2008) 845–854.
[12] D. Pech, M. Brunet, H. Durou, P. Huang, V. Mochalin, Y. Gogotsi, et al., Ultra-high-power micrometre-sized supercapacitors based on onion-like carbon, Nat. Nanotechnol. 5 (2010) 651–654.
[13] N. Behabtu, C.C. Young, D.E. Tsentalovich, O. Kleinerman, X. Wang, A.W. Ma, et al., Strong, light, multifunctional fibers of carbon nanotubes with ultrahigh conductivity, Science 339 (2013) 182–186.
[14] G. Sun, X. Zhang, R. Lin, J. Yang, H. Zhang, P. Chen, Hybrid fibers made of molybdenum disulfide, reduced graphene oxide, and multi-walled carbon nanotubes for solid-state, flexible, asymmetric supercapacitors, Angew. Chem. Int. Ed. 54 (2015) 4651–4656.
[15] S. Namgung, K.Y. Baik, J. Park, S. Hong, Controlling the growth and differentiation of human mesenchymal stem cells by the arrangement of individual carbon nanotubes, ACS Nano 5 (2011) 7383–7390.
[16] S.S. He, J.Y. Cao, S.L. Xie, J. Deng, Q. Gao, L.B. Qiu, et al., Stretchable supercapacitor based on a cellular structure, J. Mater. Chem. A 4 (2016) 10124–10129.
[17] J. Park, D. Hong, D. Kim, K.E. Byun, S. Hong, Anisotropic membrane diffusion of human mesenchymal stem cells on aligned single-walled carbon nanotube networks, J. Phys. Chem. C 118 (2014) 3742–3749.
[18] Z.M. Tao, P.Z. Wang, L. Wang, L. Xiao, F.Z. Zhang, J. Na, Facile oxidation of superaligned carbon nanotube films for primary cell culture and genetic engineering, J. Mater. Chem. B 2 (2014) 471–476.
[19] X.L. Chen, L.B. Qiu, J. Ren, G.Z. Guan, H.J. Lin, Z.T. Zhang, et al., Novel electric double-layer capacitor with a coaxial fiber structure, Adv. Mater. 25 (2013) 6436–6441.
[20] Q.W. Li, X.F. Zhang, R.F. DePaula, L.X. Zheng, Y.H. Zhao, L. Stan, et al., Sustained growth of ultralong carbon nanotube arrays for fiber spinning, Adv. Mater. 18 (2006) 3160–3163.
[21] A.A. Kuznetsov, A.F. Fonseca, R.H. Baughman, A.A. Zakhidov, Structural model for dry-drawing of sheets and yarns from carbon nanotube forests, ACS Nano 5 (2011) 985–993.
[22] J.N. Zhao, Q.S. Li, B. Gao, X.H. Wang, J.Y. Zou, S. Cong, et al., Vibration-assisted infiltration of nano-compounds to strengthen and functionalize carbon nanotube fibers, Carbon 101 (2016) 114–119.
[23] S. Li, X.H. Zhang, J.N. Zhao, F.C. Meng, G. Xu, Z.Z. Yong, et al., Enhancement of carbon nanotube fibres using different solvents and polymers, Compos. Sci. Technol. 72 (2012) 1402–1407.
[24] A. Mogilner, B. Rubinstein, The physics of filopodial protrusion, Biophys. J. 89 (2005) 782–795.
[25] A.J. Ridley, Life at the leading edge, Cell 145 (2011) 1012–1022.
[26] M. Nemethova, S. Auinger, J.V. Small, Building the actin cytoskeleton: filopodia contribute to the construction of contractile bundles in the lamella, J. Cell Biol. 180 (2008) 1233–1244.
[27] Y. Zhang, W. Bai, X. Cheng, J. Ren, W. Weng, P. Chen, et al., Flexible and stretchable lithium-ion batteries and supercapacitors based on electrically conducting carbon nanotube fiber springs, Angew. Chem. Int. Ed. 53 (2014) 14564–14568.
[28] Z. Cai, L. Li, J. Ren, L. Qiu, H. Lin, H. Peng, Flexible, weavable and efficient microsupercapacitor wires based on polyaniline composite fibers incorporated with aligned carbon nanotubes, J. Mater. Chem. A 1 (2013) 258–261.
[29] D.S. Yu, K. Goh, H. Wang, L. Wei, W.C. Jiang, Q. Zhang, et al., Scalable synthesis of hierarchically structured carbon nanotube-graphene fibres for capacitive energy storage, Nat. Nanotechnol. 9 (2014) 555–562.
[30] F. Gao, L. Viry, M. Maugey, P. Poulin, N. Mano, Engineering hybrid nanotube wires for high-power biofuel cells, Nat. Commun. 1 (2010) 2.
[31] S. Bose, T. Kuila, A.K. Mishra, R. Rajasekar, N.H. Kim, J.H. Lee, Carbon-based nanostructured materials and their composites as supercapacitor electrodes, J. Mater. Chem. 22 (2012) 767–784.
[32] J. Lin, C. Zhang, Z. Yan, Y. Zhu, Z. Peng, R.H. Hauge, et al., 3-Dimensional graphene carbon nanotube carpet-based microsupercapacitors with high electrochemical performance, Nano Lett. 13 (2013) 72–78.